Finite-size scaling in band ferromagnets with non-universal critical behavior

2009 J. Phys.: Condens. Matter 21 426002

(http://iopscience.iop.org/0953-8984/21/42/426002)

J. Phys.: Condens. Matter **21** (2009) 426002 (8pp) doi:10.1088/0953-8984/21/42/426002

Finite-size scaling in band ferromagnets with non-universal critical behavior

S N Kaul and G A Basheed

School of Physics, University of Hyderabad, Central University PO, Hyderabad-500 046, Andhra Pradesh, India

E-mail: kaulsp@uohyd.ernet.in

Received 28 June 2009, in final form 31 August 2009
Published 29 September 2009
Online at stacks.iop.org/JPhysCM/21/426002

Abstract

The ultra-high sensitivity of the ferromagnetic resonance (FMR) technique has been fully exploited to study the finite-size effects in the critical region near the ferromagnetic to paramagnetic phase transition in $Cr_{75-x}Fe_{25+x}$ ($x = 0, 5$) thin films of high structural and magnetic quality. Conclusive experimental evidence is provided for the validity of finite-size scaling. Irrespective of the film thickness and composition, the critical exponents β, γ and ν for spontaneous magnetization, initial magnetic susceptibility and spin–spin correlation length retain their bulk values so that no dimensionality crossover occurs within the film thickness range covered in the FMR experiments. The present results indicate that (i) like $Cr_{75-x}Fe_{25+x}$, the previously studied Fe, Co, Ni, and $CoNi_3$ thin films behave as itinerant-electron (band) ferromagnets in which the isotropic long-range interactions between spins decay as $J(r) \sim r^{-(d+\sigma)}$ ($\sigma > 0$), and (ii) the lattice dimensionality d, spin dimensionality m, and range of spin–spin interactions (via the material-specific parameter σ) decide the (non-universal) values of the critical exponents.

1. Introduction

Thermodynamic properties near the magnetic phase transition in a d-dimensional system (*finite* in one of the dimensions and of *infinite extent* in the remaining $d - 1$ dimensions) has captured the attention of theorists for a long time; see [1–3], for reviews. However, this fascinating field became accessible to experiments only recently, when advances in the preparation techniques made it possible to grow high-quality ultrathin films. In ferromagnetic (FM) systems of infinite size, the spin–spin correlation length, ξ, diverges at the critical point $T_C(\infty)$ as $\xi = \xi_o|\epsilon|^{-\nu}$, where $\epsilon = [T - T_C(\infty)]/T_C(\infty)$ and ν is the critical exponent. The finite thickness $t = na$ (where a is a monolayer thickness or lattice spacing) of films limits the divergence of ξ and thereby causes a thickness-dependent shift in the critical temperature of a thin film of n monolayers $T_C(n)$, with respect to $T_C(\infty)$. Experimentally, one measures the thickness-induced fractional shift in T_C

$$\epsilon_n = [T_C(\infty) - T_C(n)]/T_C(\infty) = C/n^{\lambda'} \qquad (1)$$

with C a constant and λ' the shift exponent. Finite-size scaling theories [1–3] relate λ' to the correlation length exponent ν as $\lambda' = 1/\nu$. The exponent λ' thus characterizes the asymptotic critical behavior of thick films in the limit $n \to \infty$. Thickness-dependent T_C measurements [4–14] have shown that equation (1) is obeyed in a variety of FM thin films but λ' ranges between 1.0 and 1.4, 0.94 and 1.44, 1.0 and 1.49, and 1.4 and 1.6 for Fe [4–6], Ni [6, 8–11], $CoNi_3$ [6, 12] and Gd [6, 13, 14] thin films. Since these values of λ' encompass the values $\lambda' = 1/\nu = 1/0.7048 = 1.419$, $\lambda' = 1/0.6294 = 1.5884$ and $\lambda' = 1/1.0 = 1.0$ theoretically predicted [15, 16] for the $d = 3$ isotropic nearest-neighbor (nn) Heisenberg ($d = 3$, $m = 3$), $d = 3$ nn Ising ($d = 3$, $m = 1$) and $d = 2$ nn Ising ($d = 2$, $m = 1$) models, the basic issue of the universality class (represented by the lattice dimensionality, d, and order parameter dimensionality, m) to which each of these thin film systems belongs remains unresolved. The knowledge of universality class is crucial to understanding the nature and origin of magnetic order present in a given system. The dispersion in the reported values of λ' can be traced back to the fact that equation (1) has been fitted to the $T_C(n)$ data taken over a film thickness range where the dimensionality crossover occurs (i.e., either d or m or both change). Another important point to note is that the universality class cannot be unambiguously determined based on the value of a single critical exponent, such as ν.

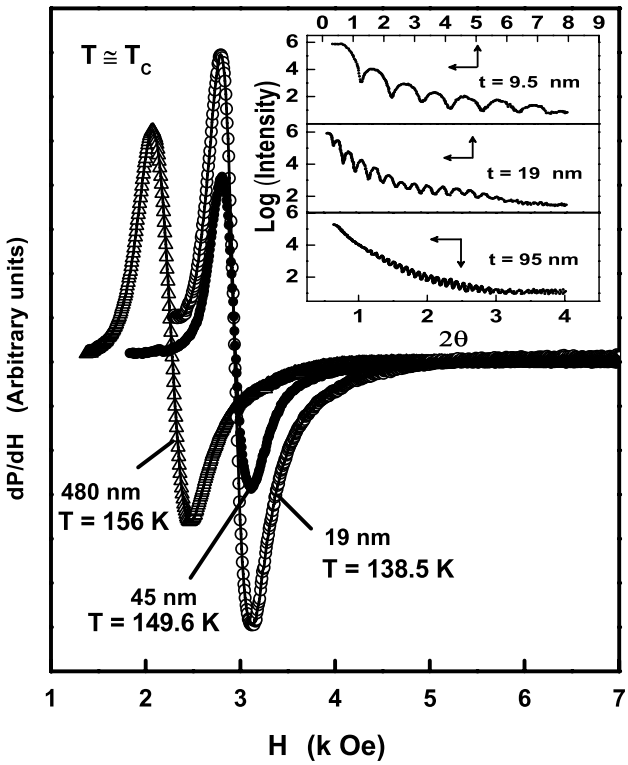

Figure 1. Field (H) dependence of the microwave power absorption derivative ($\mathrm{d}P/\mathrm{d}H$) at $T \simeq T_C$ for the $Cr_{70}Fe_{30}$ thin films of thickness $t = 19$, 45 and 480 nm. The continuous curves through the data points (symbols) denote the theoretical lineshapes. The inset displays representative small-angle x-ray scattering patterns.

To avoid complications due to the dimensionality crossover effects in finite-size scaling analysis, we measured $T_C(n)$ in ferromagnetic $Cr_{75-x}Fe_{25+x}$ ($x = 0$, 5) thin films because this alloy system, in the bulk itself, behaves as a $d = 2$, $m = 1$ ferromagnet [17] in which the attractive isotropic 'long-range' (ILR) interactions between spins decay with distance (r) as [18] $J(r) \sim r^{-(d+\sigma)}$ with $\sigma = 1.4$. We provide a rigorous experimental proof for finite-size scaling in $Cr_{75-x}Fe_{25+x}$ thin films and rationalize the λ' values reported for Fe, Co and Ni thin films in terms of a theoretical model [18] for an itinerant-electron ferromagnet with ILR spin–spin interactions of the form $J(r) \sim r^{-(d+\sigma)}$, whose critical behavior near the ferromagnetic (FM)–paramagnetic (PM) phase transition is characterized by *non-universal* critical exponents that depend on the range of interactions between spins through the *material-specific* parameter σ, which, in turn, depends on n via the lattice dimensionality, d.

2. Synthesis, characterization and experimental details

$Cr_{75-x}Fe_{25+x}$ ($x = 0$, 5) thin films of nominal thickness 500, 80, 40, 20 and 8 nm were grown on 100 μm thick glass substrates by 1 keV Ar ion-beam sputtering from a $2'' \times 2''$ target of composition $Cr_{75}Fe_{25}$ or $Cr_{70}Fe_{30}$ made out of the starting materials Cr and Fe of 99.998% purity. The temperature of the substrate (placed in a vacuum chamber evacuated to $\sim 10^{-9}$ mbar before sputtering) was maintained constant at 350 K. With an Ar gas pressure of 10^{-4} mbar during sputtering, a typical deposition rate 1.0 Å s^{-1} was achieved. During the growth process, the film thickness was monitored by a quartz crystal oscillator. Before sputtering, the targets were ion-beam milled to remove the surface oxidation layer. No deviation from the nominal composition within the uncertainty limits of ± 0.1 at.% Cr or Fe could be detected from the wavelength dispersive x-ray fluorescence compositional analysis of thick films ($t \sim 0.5$–1 μm). Wide-angle (Cu Kα) x-ray diffraction patterns revealed that the films are polycrystalline with body-centered-cubic structure (lattice parameter $a = 0.2875(5)$ nm) and have $\langle 110 \rangle$ texture along the growth direction. Standard analysis of the small-angle x-ray scattering (SAXS) data (Co Kα: $\lambda = 1.7902$ Å), shown in the inset of figure 1, yielded the actual (mean) thickness of the films as $t = 480$, 95, 45, 19 and 9.5 nm with a surface roughness $\cong 2\%$ of t. Regular oscillations in the SAXS data assert that the films are of high structural quality. Representative atomic force micrographs (taken on the films of thickness 95 and 480 nm), shown in figure 2, confirm this order of surface roughness and columnar grain growth along the film normal.

High-resolution ferromagnetic resonance measurements (in which even a few Oersted shift in the resonance field could be detected with ease) on thin films of composition $Cr_{75}Fe_{25}$

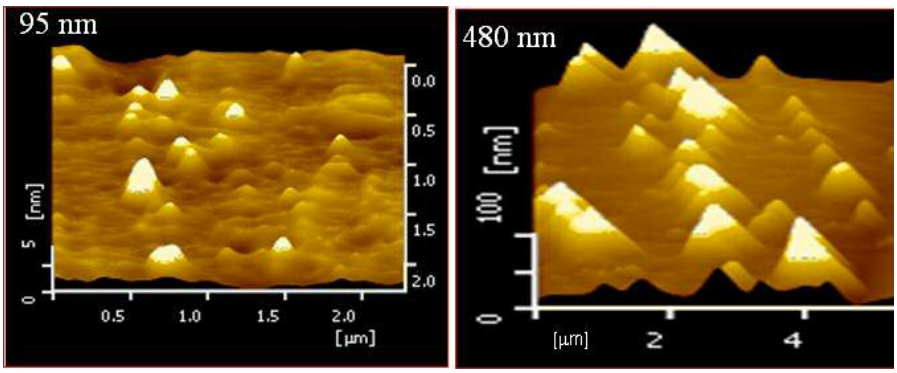

Figure 2. Typical atomic force micrographs for the $Cr_{70}Fe_{30}$ films with thickness 95 and 480 nm.
(This figure is in colour only in the electronic version)

and $Cr_{70}Fe_{30}$ were performed in the critical region near the FM–PM phase transition. To achieve high sensitivity even in ultrathin metallic films, the standard practice [19, 20] of mounting the films at the end-wall of a cylindrical microwave cavity, which is coupled to a rectangular metallic waveguide, was followed. The sensitivity of the ferromagnetic resonance technique is primarily limited by the linewidth. For a linewidth of $\Delta H_{pp}(T) \approx 1$ kOe, the detection limit is $\approx 10^{15}$ magnetic moments, which corresponds to about 3 ML cm^{-2} [20]. A copper-constantan thermocouple was used to measure temperature at the sample site.

In this paper, the results on $Cr_{70}Fe_{30}$ thin films alone are presented since the films of composition $x = 0$ and 5 essentially yield identical results. The only exception is figure 8, where the $T_C(n)/T_C(\infty)$ results for both the compositions are presented.

3. Results and discussion

Identifying T_C with the temperature at which a sharp peak in $\chi''(T)$ (the imaginary component of ac susceptibility) occurs, dP/dH versus H curves (P denotes the microwave power absorbed during the ferromagnetic resonance (FMR) process and H the steady magnetic field, applied in the film plane) were recorded on disc-shaped thin film samples, 5 mm in diameter, at a fixed microwave field frequency of $\nu = 9.27$ GHz in the temperature intervals $T_C \pm 1.5$ K, $T_C \pm 5$ K and $T_C \pm 10$ K at $\leqslant 0.1$ K, $\cong 0.5$ K and $\cong 1$ K steps, respectively. An elaborate lineshape analysis [21], based on the Landau–Lifshitz–Gilbert (LLG) equation of motion for magnetization

$$\frac{d\mathbf{M}}{dt} = -\gamma(\mathbf{M} \times \mathbf{H}_{eff}) + \frac{\lambda}{\gamma M^2(T)}\left(\mathbf{M} \times \frac{d\mathbf{M}}{dt}\right) - \frac{2A\gamma}{M^2(T)}(\mathbf{M} \times \nabla^2\mathbf{M}), \quad (2)$$

closely reproduces the observed (dP/dH)–H curves, as illustrated by figure 1, in which the continuous curves represent the theoretical LLG lineshape and symbols the dP/dH versus H data taken on the $Cr_{70}Fe_{30}$ thin films with $t = 19$ nm, 45 nm and 480 nm at $T \cong T_C$. The FMR lineshape analysis determines accurately [21] the resonance field, $H_{res}(T)$, 'peak-to-peak' FMR linewidth, $\Delta H_{pp}(T)$, magnetization, $M(T)$, and the Landé splitting factor, g. In equation (2), $\mathbf{M}$ is the sum of static and dynamic magnetizations; the effective field $\mathbf{H}_{eff} = \mathbf{H}$ (applied static magnetic field) + $\mathbf{h}(t)$ (microwave field) + $\mathbf{H}_{dem}$(demagnetizing field) + $\mathbf{H}_A$ (anisotropy field); M denotes the component of magnetization along H; $\gamma = g\mu_B/\hbar$ is the gyromagnetic ratio; λ is the Gilbert damping parameter and A is the exchange stiffness constant. In the present case, $H_{dem} = H_A \approx 0$ and $h(t) \ll H$. The first term on the right-hand side of equation (2) is the torque exerted by $\mathbf{H}_{eff}$ on $\mathbf{M}$, whereas the second and third terms represent the torques due to the Gilbert damping and the effective exchange field, $\mathbf{H}_{ex} = (2A/M^2)\nabla^2\mathbf{M}$. The latter two torques govern the relaxation towards equilibrium. $\mathbf{H}_{ex}$ does not point in the direction of $\mathbf{M}$ because the finite penetration of the microwave field makes the orientation of $\mathbf{M}$ *non-uniform* in the skin depth of a ferromagnetic metal.

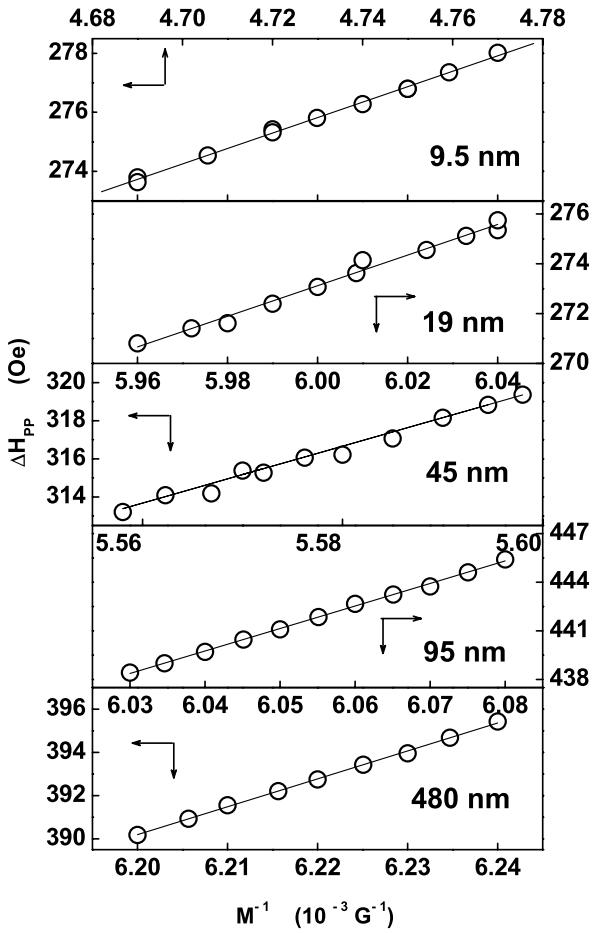

Figure 3. Linear variation of the 'peak-to-peak' FMR linewidth, ΔH_{pp}, with inverse magnetization, M^{-1}. Arrows indicate the relevant ordinate and abscissa scales.

Equation (2) yields $\Delta H_{pp}(T)$ as a sum of the contributions arising from two-magnon scattering processes [22] (grain–grain and/or grain-boundary two-magnon scattering caused by local magnetic inhomogeneities), Gilbert damping [23] $\Delta H_{LLG}(T) = (2/\sqrt{3})(\lambda\omega/\gamma^2 M(T))$, and the exchange-conductivity (EC) mechanism [23] $\Delta H_{EC}(T) = (16\pi/3)(\sqrt{A(T)\omega/\rho(T)}/c)$, where ρ and c respectively stand for the electrical resistivity and velocity of light. As the temperature is raised towards T_C, M and exchange stiffness $A(T) \sim [M(T)]^2$ decrease (the rate of decline becomes very steep as $T \to T_C$) and have a small magnitude at $T = T_C$, while resistivity, ρ, increases with temperature and attains relatively large values at $T \approx T_C$. Consequently, the LLG contribution, $\Delta H_{LLG}(T) \sim [M(T)]^{-1}$, is expected to completely swamp the EC contribution, $\Delta H_{EC}(T) \sim M(T)/\sqrt{\rho(T)}$, and essentially determine $\Delta H_{pp}(T)$ in a narrow temperature range below T_C. That this is indeed the case in the range $-10^{-2} \leqslant \epsilon_t = [T - T_C(t)]/T_C(t) \leqslant -10^{-4}$ (the critical region) is demonstrated by the data presented in figure 3. The slope $= (2\omega/\sqrt{3}\gamma^2)\lambda$ of the linear ΔH_{pp}–M^{-1} plots (figure 3) permits an accurate determination of the Gilbert damping parameter, λ. From the λ–$(1/t)$ plot shown in figure 4, it is evident that λ drops to nearly 50% of its bulk value $(0.42(1) \times 10^8\ s^{-1})$ at $t = 480$ nm, whereas from

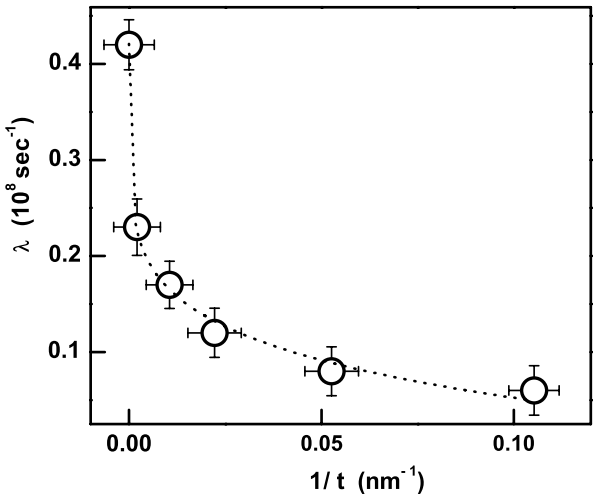

Figure 4. Gilbert damping parameter, λ, versus inverse thickness.

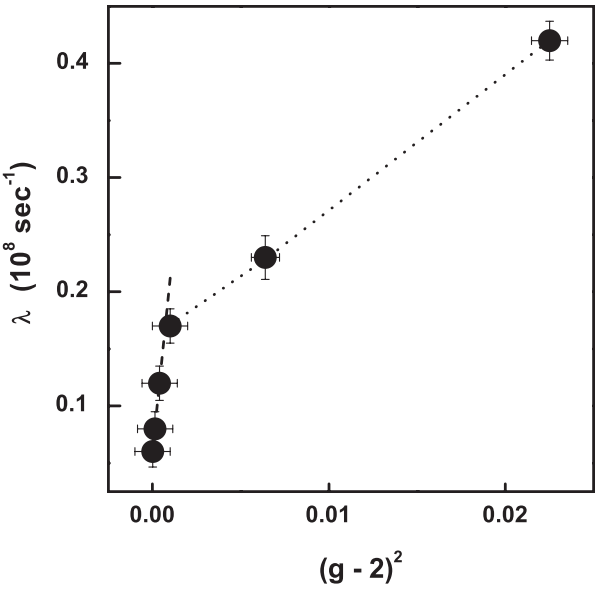

Figure 5. Linear variation of λ with $(g-2)^2$. The dotted curves serve as a guide to the eye.

$t = 480$ to 9.5 nm λ drops by 73%. For $T \approx T_C$, spin–spin interactions are expected to be weak with the result spin–lattice interactions (via spin–orbit coupling) dominantly contribute to damping and decide the Landé g factor. The assumption that the spin–lattice relaxation is the sole damping mechanism leads to the theoretical result [24]: $\lambda \sim (g-2)^2(\Theta_D/T)^2$ if $T \ll \Theta_D$. Figure 5 shows that this proportionality between λ and $(g-2)^2$ holds over a certain thickness regime. Outside the critical region, the FMR linewidth is mainly governed by the exchange-conductivity mechanism with the result that $\Delta H_{pp}(T) \cong \Delta H_{EC}(T)$, as is borne out by the dashed curves in figure 6. As expected, the exchange-conductivity contribution becomes increasingly important in thicker films so that the LLG contribution governs $\Delta H_{pp}(T)$ over a larger temperature range as the film thickness, t, decreases (figure 6).

ΔH_{pp} is known to be extremely sensitive [25] to the structural and magnetic quality of metallic thin films. The

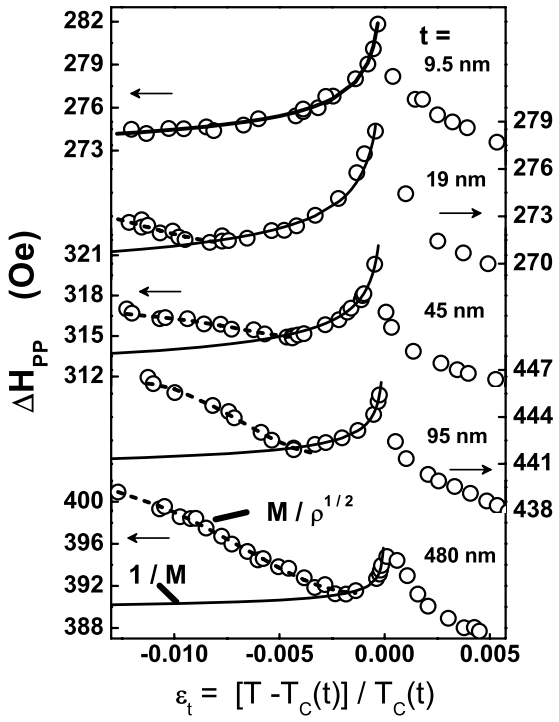

Figure 6. $\Delta H_{pp}(T)$ in the temperature interval $-0.012 \lesssim \epsilon_t \lesssim 0.005$. The continuous and dashed curves depict the temperature variations $\Delta H_{pp}(\epsilon_t) = a + b(-\epsilon_t)^{-\beta}$ and $\Delta H_{EC}(T) \sim M(T)/\sqrt{\rho(T)}$.

narrowest FMR linewidths, ranging between 200 and 500 Oe, have been observed [25] outside the critical region in exceptionally high-quality films epitaxially grown under ultra-high vacuum conditions. The finding that, depending upon the film thickness, $\Delta H_{pp}(T)$ ranges between 270 and 440 Oe (figures 3 and 6) at temperatures away from the peak testifies to the high structural and magnetic quality of the investigated films.

The sharp cusp in $\Delta H_{pp}(T)$ occurs at the same temperature ($\cong T_C$) at which χ'' peaks. Since the magnetization, $M(T, H_{res})$, measured in the FMR experiment, does not differ appreciably from the spontaneous magnetization, $M_S(T)$, the relation $\Delta H_{LLG}(T) \sim [M(T)]^{-1}$, valid in the critical region, permits an estimation of the critical exponent β for the order parameter, $M_S(T)$, via its modified form $\Delta H_{pp}(\epsilon_t) = a + b(-\epsilon_t)^{-\beta}$. Optimum fits (continuous curves in figure 6) to the $\Delta H_{pp}(T)$ data, based on this relation, yield $\beta = 0.30(1)$ irrespective of the film thickness, and $T_C(t)$ values that match those deduced from $\chi''(T)$ to within ±0.1 K.

Such estimates for the critical exponent β have to be regarded as rough, since the peak value of the ΔH_{pp} differs from the back ground (270–440 Oe) by only 6–9 Oe. A weak but sharp cusp in $\Delta H_{pp}(T)$ at $T \cong T_C$ strongly indicates that only a small fraction of the total number of spins is actually participating in the FM–PM phase transition. To obtain highly precise estimates for $T_C(t)$ and true asymptotic values of the critical exponents β and γ for spontaneous magnetization and initial magnetic susceptibility, we follow the approach detailed elsewhere [26]. In this approach, H_{res} is identified

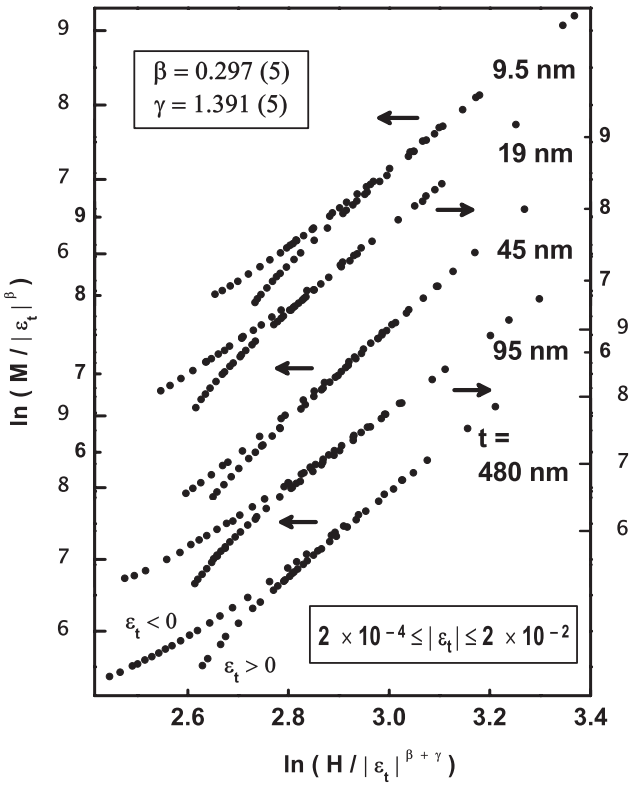

Figure 7. $(M/|\epsilon_t|^{\beta})$ versus $(H/|\epsilon_t|^{\beta+\gamma})$ scaling plots. Note that the outer (inner) ordinate scales correspond to the films of thickness 9.5, 95 and 480 nm (19 and 45 nm).

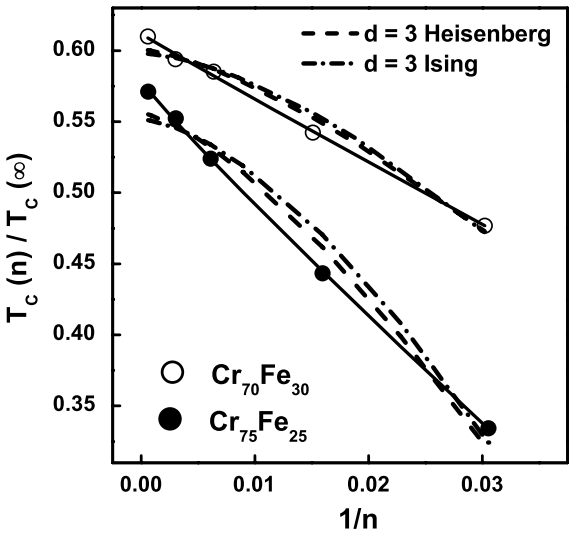

Figure 8. Finite-size scaling of the film thickness-dependent T_C. The dashed and dash–dotted curves represent the variations predicted by the $d = 3$ Heisenberg and $d = 3$ Ising models, respectively.

with the ordering field H conjugate to magnetization M and consistent with the scaling equation of state (SES) $m_t = f_{\pm}(h_t)$ (where $m_t \equiv M/|\epsilon_t|^{\beta}$ and $h_t \equiv H/|\epsilon_t|^{\beta+\gamma}$ are the scaled magnetization and scaled field), and the $M(T, H) \equiv M(T, H_{\rm res})$ data, in the critical region, are made to fall [27] on two universal curves, f_- for $\epsilon_t < 0$ and f_+ for $\epsilon_t > 0$, through an appropriate choice of the parameters $T_C(t)$, β and γ. Next, use is made of the 'range-of-fit' SES analysis in which more and more of the data taken at temperatures away from $T_C(t)$ are excluded from the m_t–h_t plot so that the exponents β and γ become increasingly sensitive to the value of $T_C(t)$ and strong departures [28] from the curves $f_-(h_t)$ and $f_+(h_t)$ occur if the choice of β and γ differs even slightly from the correct one. This procedure, thus, goes on refining [26–28] the estimates of β and γ till their *asymptotic* values are reached.

The $\ln m_t$–$\ln h_t$ plots for the $Cr_{70}Fe_{30}$ films in the asymptotic critical region $2 \times 10^{-4} \leqslant |\epsilon_t| \leqslant 2 \times 10^{-2}$ are shown in figure 7. The asymptotic values $\beta = 0.297(5)$, $\gamma = 1.391(5)$ for the critical exponents β and γ, so determined, are *independent of film thickness* and *composition*. In table 1, these exponent values are compared with those reported [17, 29–31] previously for $Cr_{75}Fe_{25}$ and $Cr_{70}Fe_{30}$ bulk samples and with the theoretical estimates [32–34][1] for $d = 2$ or 3 ferromagnets with either short-range exchange interactions [32, 33] or isotropic long-range dipolar interactions [34] or isotropic long-range (ILR) exchange interactions decaying with interspin distance, r, as $J(r) \sim r^{-(d+\sigma)}$ with $0 < \sigma < 2$. Another theoretical result, which could have an important bearing, is that the asymptotic critical exponents of a ferromagnetic model on a simple cubic lattice with Ruderman–Kittel–Kasuya–Yosida (RKKY) interactions are the same [35] as those of the corresponding nearest-neighbor (short-range) model. The comparison made in table 1 reveals the following. (a) Even in thin films, the critical exponents β and γ retain their bulk values. (b) Though the experimentally determined value $\gamma = 1.390(5)$ is fairly close to $\gamma = 1.386(4)$ ($\gamma = 1.372$) theoretically predicted for the $d = 3$ isotropic short-range (ISR) Heisenberg ($d = 3$ isotropic dipolar) ferromagnet, the observed value $\beta = 0.298(5)$ lies far below the corresponding theoretical estimate $\beta = 0.365(2)$ ($\beta = 0.381$). (c) The experimental values of the exponents β and γ do not correspond to any known universality class but tally quite well with the values[1] $\beta = 0.298$ and $\gamma = 1.392$, predicted by the renormalization group (RG) theory [18] for a $d = 2$, $m = 1$ ferromagnet with ILR interactions between spins of the form $J(r) \sim r^{-(d+\sigma)}$ with $\sigma = 1.4$. Note that no choice of σ in the permissible range $(d/2) < \sigma \leqslant 2$ for a $d = 3$, $m = 3$ or $d = 2$, $m = 2$ or $d = 3$, $m = 1$ ferromagnet reproduces the observed values of the critical exponents.

Previous determinations [6, 8–14] of the thickness-induced shift in the T_C of Fe, Co, Ni and Gd thin films have revealed that the bulk value of T_C is retained for thicknesses down to ≈30 monolayers but T_C drops rapidly when the thin film thickness falls below 8–10 monolayers. In sharp contrast with this usual behavior, in $Cr_{75-x}Fe_{25+x}$ thin films, T_C drops to 57% (61%) of its bulk value [17] $T_C(\infty) = 145.01(1)$ K ($T_C(\infty) = 256.00(1)$ K) at a thickness as large as $t = 480$ nm or $n \simeq 1670$ monolayers in the alloy with $x = 0$ ($x = 5$) and, from a thickness of $t = 480$ to 9.5 nm or $n = 33$ monolayers, T_C decreases by only ≅41% (≅22%). However,

[1] The parameter σ is chosen such that the expression for the critical exponent γ given in [18] yields a value (≃1.39) close to that observed experimentally and the remaining critical exponents are calculated by inserting the value of γ, so obtained, in the expression $\nu = \gamma/\sigma$, and by using the scaling equalities $\alpha = 2 - \nu d$, $\beta = (2 - \alpha - \gamma)/2$ and $\delta = 1 + (\gamma/\beta)$.

Table 1. Comparison between experiment and theory. Abbreviations: AA—asymptotic analysis; ACS—AC susceptibility; B—bulk; BM—bulk magnetization; FMR—ferromagnetic resonance; FSS—finite-size scaling; MAP—modified Arrott plot analysis; PC—polycrystalline; RG-ϕ^4—renormalization group ϕ^4 field theory; RG-ϵ—renormalization group epsilon ($\epsilon = 4 - d$) expansion; RG-ϵ'—renormalization group epsilon ($\epsilon' = 2\sigma - d$) expansion; SANS—small-angle neutron scattering; SC—single crystal; SES—scaling equation of state analysis; t—thickness; TF—thin film.

Experiment/theory	Reference	Method	β	γ	δ	ν	Remarks
Experiment							
$Cr_{75}Fe_{25}$	[17]	BM, MAP, SES	0.300(10)	1.390(10)	5.50(10)		B, PC
$Cr_{75}Fe_{25}$	[29]	ACS, AA		1.360(30)			B, PC
$Cr_{75}Fe_{25}$	[30]	ACS, SES	0.305(15)	1.330(60)	5.46(15)		B, SC
$Cr_{75}Fe_{25}$	This work	FMR, SES, FSS	0.298(4)	1.389(6)		1.07(8)	TF, 9.5 nm $\leqslant t \leqslant$ 480 nm
$Cr_{75}Fe_{25}$	[31]	SANS				1.20(10)	B, PC
$Cr_{70}Fe_{30}$	[17]	BM, MAP, SES	0.315(5)	1.390(10)	5.36(4)		B, PC
$Cr_{70}Fe_{30}$	[29]	ACS, AA		1.390(30)			B, PC
$Cr_{70}Fe_{30}$	[29]	BM, MAP, SES	0.307(5)	1.390(10)	5.56(5)		TF, t = 9.4 nm
$Cr_{70}Fe_{30}$	This work	FMR, SES, FSS	0.297(5)	1.391(5)		1.04(8)	TF, 9.5 nm $\leqslant t \leqslant$ 480 nm
Theory							
Short-range exchange: $J(r) \sim e^{-r/b}$							
$d = 2,\ m = 1$	[32]	Onsager solution	0.125	1.75	15.0	1.0	Exact result
$d = 3,\ m = 1$	[15, 16, 33]	RG-ϕ^4	0.325(2)	1.241(2)	4.82(3)	0.630(2)	
$d = 3,\ m = 2$	[15, 16, 33]	RG-ϕ^4	0.346(2)	1.316(3)	4.81(3)	0.669(2)	
$d = 3,\ m = 3$	[15, 16, 33]	RG-ϕ^4	0.365(2)	1.386(4)	4.80(4)	0.705(3)	
Isotropic long-range dipolar							
$d = 3,\ m = 3$	[34]	RG-ϵ	0.381	1.372	4.45	0.692	
Isotropic long-range exchange: $J(r) \sim r^{-(d+\sigma)}$							
$d = 2,\ m = 1,\ \sigma = 1.4$	(See footnote 1)	RG-ϵ'	0.298	1.392	5.67	1.00(1)	Compare with experimental values
$d = 2,\ m = 2,\ \sigma = 1.325$	(See footnote 1)	RG-ϵ'	0.354	1.389	4.93	1.05(1)	
$d = 2,\ m = 3,\ \sigma = 1.285$	(See footnote 1)	RG-ϵ'	0.386	1.389	4.59	1.08(1)	

when $T_C(n)/T_C(\infty)$ is plotted against $1/n$ (with $n = t/a$), as shown in figure 8, equation (1), represented by the continuous line, closely reproduces the $T_C(n)$ data over the thickness range extending from $n = 33$ ($t = 9.5$ nm) to $n = 1672$ ($t = 480$ nm), with $\lambda' = 0.93(7)$ and $\lambda' = 0.96(7)$ or, equivalently, $\nu = 1.07(8)$ and $\nu = 1.04(8)$ for the alloys with $x = 0$ and $x = 5$, respectively. By comparison, the $d = 3$, $m = 3$ (dashed curves) and $d = 3$, $m = 1$ (dotted curves) short-range models fail to describe the observed variations of $T_C(n)/T_C(\infty)$ with $1/n$. The values $\nu = 1.07(8)$ and 1.04(8) compare very well with $\nu = 0.99(1)$, obtained from the relation [18] $\nu = \gamma/\sigma$ when the values $\gamma = 1.391(5)$ and $\sigma = 1.4$ are used, and also with the value $\nu = 1.2(1)$ determined from the small-angle neutron scattering [31] data on bulk $Cr_{75}Fe_{25}$. A perfect agreement between the values of the critical exponents β, γ and ν for the $Cr_{75-x}Fe_{25+x}$ ($x = 0$, 5) alloys in the bulk and thin film forms, and between the currently determined and theoretically predicted exponent values for the $d = 2$, $m = 1$ ferromagnet with interspin interactions of the form $J(r) \sim r^{-3.4}$, asserts that, even in the bulk, long-range ferromagnetic order is sustained by such long-range spin–spin interactions. A steep drop in T_C and λ from their bulk values as the film thickness reduces to $t = 480$ nm basically reflects diminished spin–spin interactions due to lesser neighbors for a given spin in the ramified spin network of reduced spatial dimensionality [17] of $d \simeq 2$. This inference is consistent with the earlier deduction from the cusp in $\Delta H_{pp}(T)$ that only a small fraction of spins is involved in the FM–PM phase transition.

In order to understand why even for the *bulk* $Cr_{75-x}Fe_{25+x}$ ($x = 0$, 5) alloys the lattice dimensionality is 2 rather than 3, we need to draw upon the well-documented magnetic phase diagram [36] of the bulk $Cr_{100-c}Fe_c$ system, determined by small-angle neutron scattering (SANS), low-field magnetization (LFM) and ac susceptibility (ACS). According to this phase diagram, $Cr_{100-c}Fe_c$ alloys exhibit itinerant antiferromagnetism, spin glass behavior and itinerant ferromagnetism in the Fe concentration regimes $c \leqslant c_{AF} \cong 16$ at.%, 16 at.% $\leqslant c \leqslant 19$ at.% and $c \geqslant c_{FM} \cong 20$ at.%. SANS results provided a direct evidence for a slow evolution of a homogeneous ferromagnetic (FM) order from an extremely inhomogeneous (non-collinear) FM order near c_{FM} (the critical concentration for the appearance of FM order) as c is increased from c_{FM}; a long-range collinear FM order emerged only for $c > 30$ at.% Fe. These observations found a qualitative interpretation in terms of a percolation model [36] in which the spin system below T_C is perceived as an infinite FM percolating cluster coexisting with finite clusters. For $c \approx c_{FM} \cong 20$ at.% Fe a large fraction of spins (magnetic moments) belong to finite clusters, but as the Fe concentration is increased, more and more of the spins become part of the infinite cluster. This trend was corroborated by the intensification of the critical scattering peak, reflecting the growth of the infinite cluster, and by the concomitant reduction in the low-temperature scattering (associated with the finite cluster response in the re-entrant state, where the long-range FM order coexists with the spin glass order). Our earlier LFM and ACS results [17] on bulk $Cr_{75}Fe_{25}$ and $Cr_{70}Fe_{30}$ alloys are consistent with this

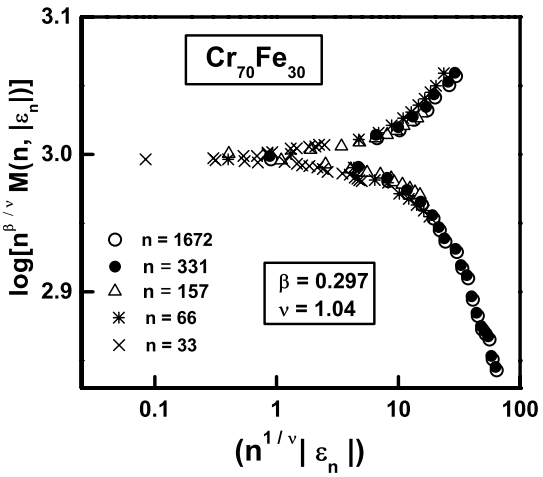

Figure 9. Finite-size scaling of the film thickness-dependent magnetization.

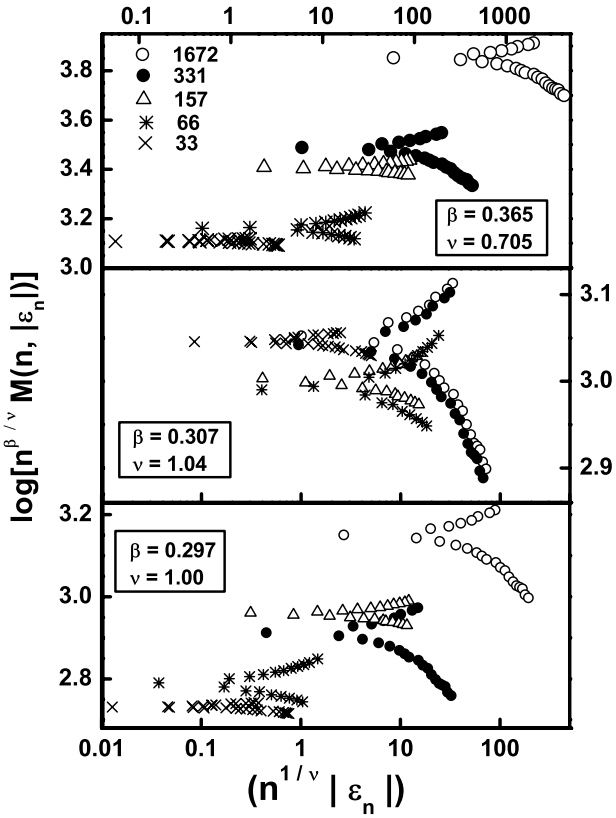

Figure 10. Breakdown of the finite-size scaling of magnetization for the values of β and ν that differ slightly from the optimum choice $\beta = 0.297$ and $\nu = 1.04$.

percolation description [17, 27]. Since these compositions are not far enough from the percolation threshold $c_{\mathrm{FM}} \cong 20$ at.%, the infinite cluster, which disorders at T_{C}, has an extremely ramified structure and hence behaves as a $d = 2$ spin system rather than $d = 3$. Note that a highly ramified infinite spin network needs a long-range interaction such as ILR interaction between spins of the form $J(r) \sim r^{-(d+\sigma)}$ with $\sigma = 1.4$ to sustain long-range ferromagnetic order.

A more stringent test for the validity of the finite-size scaling theory is provided by the requirement that the magnetization of thin films of varied thickness, n, should scale in accordance with the relation [1–3]

$$M(n, \epsilon_n) = n^{-\beta/\nu} g_{\pm}(n^{1/\nu}\epsilon_n) \tag{3}$$

where $\epsilon_n = [T - T_{\mathrm{C}}(n)]/T_{\mathrm{C}}(n)$ and the plus and minus signs refer to temperatures above and below $T_{\mathrm{C}}(n)$. That this is indeed the case is demonstrated by the $n^{\beta/\nu}M(n, \epsilon_n)$–$n^{1/\nu}\epsilon_n$ plot (shown in figure 9), constructed using the currently determined values of $M(n, T)$, $T_{\mathrm{C}}(n)$, $\beta(=0.297(5))$ and $\nu(=1.04(8))$. Note that there are no adjustable parameters in this scaling plot. The $n^{\beta/\nu}M(n, \epsilon_n)$–$n^{1/\nu}\epsilon_n$ plots in figure 10 serve to illustrate the extreme sensitivity of the finite-size scaling of magnetization to the choice of β and ν. Figure 10 clearly demonstrates that the finite-size scaling breaks down completely (i) for the $d = 3$ isotropic short-range (ISR) Heisenberg values $\beta = 0.365$ and $\nu = 0.705$ (top panel) or even for the $d = 3$ short-range Ising values (not shown), and (ii) when either β or ν differs even slightly from the optimum choice of $\beta = 0.297$ or $\nu = 1.04$. In an attempt to rationalize the previously reported [4–12] values of λ' for the Fe, Co, Ni and $CoNi_3$ thin films, cognizance has to be taken of the long-range nature [37] of spin–spin interactions in these itinerant-electron ferromagnets. One such attempt made recently [6] uses the mean-field (MF) approximation and introduces a cut-off range, N_0, of the spin–spin interactions at which a crossover from the power law, $\epsilon_n \sim n^{-\lambda'}$ (with $\lambda' = 1$) for $n \geqslant N_0$, to linear behavior, $\epsilon_n \sim n$ for $n < N_0$, occurs. Though this approach adequately describes the observed $\epsilon_n(n)$, it yields MF critical exponents that are in serious conflict [4, 5, 7–10, 12] with the experimental findings. In an attempt to resolve this contradiction, we take recourse to the renormalization group (RG) calculations [18] on a (d, m) spin system with isotropic long-range (ILR) interactions of the form $(J_\infty/r^{d+\sigma})\mathbf{S}_0\cdot\mathbf{S}_r$ that predict the following. (i) ILR interactions render the $d = 3$ Heisenberg fixed point unstable and lead to a crossover [18] to a *new* fixed point, which is characterized by *non-universal* critical exponents that depend on σ when $(d/2) < \sigma < 2$. (ii) The short-range critical behavior (essentially determined by d and m) prevails for all d when $\sigma > 2$. In a previous work [38], it has been shown that in the bulk form Ni is the experimental realization of case (i) with [38] $d = 3$, $m = 3$ and $\sigma = 1.91$. Considering Ni thin films with $7 \leqslant n \leqslant 20$ as a spin system with $d = 3$, $m = 1$ and $\sigma = 1.91$, the expression for the exponent γ and the relation $\nu = \gamma/\sigma$ given in [18] yield $\gamma = 1.23$ and $\nu = 0.64$ for such a system. Using these values in the scaling relations $\alpha = 2 - \nu d$ and $\beta = (2 - \alpha - \gamma)/2$ gives the specific heat critical exponent $\alpha = 0.07$ and $\beta = 0.35$. These values compare well with $\nu = 0.71(6)$ and $\beta = 0.32(6)$ reported [8] in the above-mentioned thickness range for Ni thin films. The above calculations, when repeated for the choice $d = 3$, $m = 3$ and $\sigma = 1.9$, yield the critical exponent values $\gamma = 1.331$, $\nu = 0.701$, $\alpha = -0.102$, $\beta = 0.385$ and $\delta = 4.45$. These values match quite well with the most accurate [27] experimental estimates $\gamma = 1.333(1)$, $\beta = 0.389(5)$ and $\delta = 4.35(5)$ reported [39] for bulk Fe so far. In the limit

$n \to 1$, $d \to 2$, $\sigma \to 2.91$ (2.9) in the exponent $(d + \sigma) = 4.91(4.9)$ of the power law $J(r) \sim r^{-(d+\sigma)}$ for Ni (Fe). Since $\sigma > 2$, case (ii) should apply for both Ni and Fe monolayer films. Consistent with this prediction, a short-range $d = 2$ Ising critical behavior has been observed in Ni [8] (Fe [4]) thin films with $n \leqslant 4$ ($n \leqslant 1$). The same arguments, albeit with a different value of σ, hold for Co and $CoNi_3$ thin films [7, 12] as well. By contrast, long-range Ruderman–Kittel–Kasuya–Yosida and dipole–dipole interactions couple the *localized* 4f magnetic moments in Gd metal [40] and lead to the sequence of crossovers: uniaxial dipolar → isotropic dipolar → Gaussian, as the temperature is raised from $T = T_C$. Studies [13, 14, 41] on the thickness-induced shift in T_C, and changes in the critical behavior near T_C, in Gd thin films reveal a crossover from $d = 3$ to 2 short-range Ising critical behavior as the film thickness reduces from 27 monolayers to $\simeq$1 monolayer. Thus, Gd thin films have to be treated on a different theoretical footing.

4. Summary and conclusion

The validity of the finite-size scaling involving the thickness-induced shift in Curie temperature as well as thickness-dependent magnetization has been demonstrated in high-quality $Cr_{75-x}Fe_{25+x}$ ($x = 0$, 5) thin films. A sharp cusp in the FMR linewidth at $T = T_C$ marks the ferromagnetic (FM) to paramagnetic (PM) phase transition even in the film of least thickness. Critical exponents β, γ and ν, characterizing the FM–PM transition, retain their bulk values $\beta = 0.297(5)$, $\gamma = 1.391(5)$ and $\nu = 1.05(8)$, irrespective of the film thickness and composition so that no dimensionality crossover occurs in the film thickness range covered in the present experiments. These critical exponent values conform very well with those [17] ($\beta = 0.298$, $\gamma = 1.392$ and $\nu = 1.0$) predicted by the renormalization group (RG) theory [18] for a $d = 2$, $m = 1$ ferromagnet in which the isotropic long-range interactions between spins decay as $J(r) \sim r^{-(d+\sigma)}$ with $\sigma = 1.4$. The RG calculations [18] are shown to provide a consistent theoretical basis for the previously reported results on the finite-size effects in itinerant-electron ferromagnets such as Fe, Co and Ni thin films. The Gilbert damping mechanism, responsible for the observed FMR linewidth in a narrow temperature range within the critical region, in the present case, has its origin in the spin–lattice relaxation.

References

[1] Barber M N 1983 *Phase Transitions and Critical Phenomena* vol 8, ed C Domb and J Lebowitz (New York: Academic) chapter 2

[2] Privman V (ed) 1990 *Finite Size Scaling and Numerical Simulation of Statistical Systems* (Singapore: World Scientific)

[3] Henkel M 1998 *Conformal Invariance and Critical Phenomena* (Heidelberg: Springer)

[4] Elmers H J, Hauschild J, Höche H, Gradman U, Bethge H, Heuer D and Köhler U 1994 *Phys. Rev. Lett.* **73** 898

[5] Henkel M, Andrieu S, Bauer P and Piecuch M 1998 *Phys. Rev. Lett.* **80** 4783

[6] Zhang R and Willis R F 2001 *Phys. Rev. Lett.* **86** 2665

[7] Schneider C M, Bressler P, Schuster P, Krischner J, de Miguel J J and Miranda R 1990 *Phys. Rev. Lett.* **64** 1059

[8] Li Y and Baberschke K 1992 *Phys. Rev. Lett.* **68** 1208

[9] Tjeng L H, Idzerda Y U, Rudolf P, Sette F and Chen C T 1992 *J. Magn. Magn. Mater.* **109** 288

[10] Tischer M, Arvanitis D, Yokoyama T, Lederer T, Tröger L and Baberschke K 1994 *Surf. Sci.* **307–309** 1096

[11] Sun L, Searson P C and Chien C L 2000 *Phys. Rev.* B **61** R6463

[12] Huang F, Mankey G J, Kief M T and Willis R F 1994 *J. Appl. Phys.* **73** 6760
Huang F, Mankey G J, Kief M T and Willis R F 1994 *Phys. Rev.* B **49** 3962

[13] Farle M, Baberschke K, Stetter U, Aspelmeier A and Gerhardter F 1993 *Phys. Rev.* B **47** 11571

[14] Jiang J S, Davidovic D, Reich D H and Chien C L 1995 *Phys. Rev. Lett.* **74** 314
Jiang J S and Chien C L 1993 *J. Appl. Phys.* **79** 5615

[15] Zinn-Justin J 1989 *Quantum Field Theory and Critical Phenomena* (Oxford: Oxford University Press) chapter 25

[16] Ferrenberg A M and Landau D P 1991 *Phys. Rev.* B **44** 5081
Chen K, Ferrenberg A M and Landau D P 1993 *Phys. Rev.* B **48** 3249

[17] Fischer S F, Kaul S N and Kronmuller H 2002 *Phys. Rev.* B **65** 06443

[18] Fisher M E, Ma S K and Nickel B G 1972 *Phys. Rev. Lett.* **29** 917

[19] Heinrich B 1994 *Ultrathin Magnetic Structures* vol II ed B Heinrich and J A C Bland (Berlin: Springer) p 195

[20] Farle M 1998 *Prog. Phys.* **61** 755

[21] Kaul S N and Siruguri V 1987 *J. Phys. F: Met. Phys.* **17** L255
Kaul S N and Siruguri V 1992 *J. Phys.: Condens. Matter* **4** 505

[22] Heinrich B, Urquhart K B, Arrott A S, Cochran J F, Myrtle K and Purcell S T 1987 *Phys. Rev. Lett.* **59** 1756

[23] Vonsovskii S V 1966 *Ferromagnetic Resonance* (Oxford: Pergamon)

[24] Elliott R J 1954 *Phys. Rev.* **96** 266

[25] Platow W, Anisimov A N, Dunifer G L, Farle M and Baberschke K 1998 *Phys. Rev.* B **58** 5611

[26] Kaul S N and Babu P D 1992 *Phys. Rev.* B **45** 295

[27] Kaul S N 1985 *J. Magn. Magn. Mater.* **53** 5

[28] Fähnle M, Kellner W U and Kronmüller H 1987 *Phys. Rev.* B **35** 3640
Kellner W U, Fähnle M, Kronmüller H and Kaul S N 1987 *Phys. Status Solidi* b **144** 397

[29] Fischer S F, Kaul S N and Kronmüller H 2001 *J. Magn. Magn. Mater.* **226–230** 540

[30] Fischer S F, Kaul S N and Kronmüller H 2004 *J. Magn. Magn. Mater.* **272–276** 254

[31] Burke S K and Rainford B D 1983 *J. Phys. F: Met. Phys.* **13** 471

[32] Fischer M E 1974 *Rev. Mod. Phys.* **46** 597

[33] LeGuillou J C and Zinn-Justin J 1980 *Phys. Rev.* B **21** 3976

[34] Bruce A D and Aharony A 1974 *Phys. Rev.* B **10** 2078

[35] Beutler R and Fähnle M 1989 *Phys. Rev.* B **40** 11417

[36] Burke S K, Cywinski R, Davis J R and Rainford B D 1983 *J. Phys. F: Met. Phys.* **13** 451

[37] Kaul S N 1983 *Phys. Rev.* B **27** 5761

[38] Seeger M, Kaul S N, Kronmüller H and Reisser R 1995 *Phys. Rev.* B **51** 12585

[39] Arajs A, Tehan B L, Anderson E E and Stelmach A A 1970 *Int. J. Magn.* **1** 41

[40] Srinath S and Kaul S N 1999 *Phys. Rev.* B **60** 12166
Srinath S, Kaul S N and Kronmüller H 1999 *Phys. Rev.* B **59** 1145

[41] Farle M and Baberschke K 1987 *Phys. Rev. Lett.* **58** 511